Materials and Structures (2022) 55:251
https://doi.org/10.1617/s11527-022-02082-9

ORIGINAL ARTICLE

Steered fiber orientation: correlating orientation and residual tensile strength parameters of SFRC

Filippo Medeghini · Jajnabalkya Guhathakurta · Giuseppe Tiberti · Sven Simon · Giovanni A. Plizzari · Peter Mark

Received: 10 August 2022 / Accepted: 20 November 2022 / Published online: 10 December 2022

Abstract Adding steel fibers to concrete improves the post-cracking tensile strength of the composite material due to fibers bridging the cracks. The residual performance of the material is influenced by fiber type, content and orientation with respect to the crack plane. The latter is a main issue in fiber-reinforced concrete elements, since it significantly influences the structural behavior. The aim of this research is to develop a tailor-made composite material and casting method to orient fibers in order to optimize the performance of the material for structural applications. To this aim, a mechanized concreting device that induces such preferred fiber orientation is designed and fabricated. It uses vibration and a series of narrow channels to guide and orient fibers. A composite with oriented fibers is produced using a hybrid system of macro and micro fibers and high-performance concrete. From the same concrete batch, specimens are cast both with and without the fiber orientation device, obtaining different levels of fiber orientation. Three-point bending tests are performed to measure and compare the residual tensile strength capacities with standard specimens cast according to EN 14651. Elements with favorable fiber orientation show a significant increase in residual tensile strength with respect to the standard beams. Finally, computed tomography and an electromagnetic induction method are employed to better assess the orientation and distribution of fibers in the beams. Their results are in good agreement and enable to link the residual tensile strength parameters with fiber orientation.

Keywords Fiber orientation · SFRC · Residual flexural tensile strength · Steering of fibers · X-ray computed tomography (CT)

Giovanni A. Plizzari, co-author of this paper, is currently deputy editor-in-chief of the journal Materials and Structures.

F. Medeghini (✉) · P. Mark
Institute of Concrete Structures, Ruhr University Bochum, Universitätsstraße 150, 44801 Bochum, Germany
e-mail: filippo.medeghini@rub.de

F. Medeghini · G. Tiberti · G. A. Plizzari
Department of Civil, Environmental, Architectural Engineering and Mathematics, University of Brescia, Piazza del Mercato 15, 25121 Brescia, Italy

J. Guhathakurta · S. Simon
Department of Computational Imaging Systems, Institute of Computer Architecture and Computer Engineering, University of Stuttgart, Universitätsstraße 38, 70569 Stuttgart, Germany

1 Introduction

Steel fiber reinforced concrete (SFRC) is a composite material which has been deeply studied in the last decades, mainly for its ability to transfer stresses across a cracked section [1–3]. Its insertion into design

codes [4, 5] opened the way to different structural applications: tunnel segments [6, 7], industrial pavements [8] and more [9], either as the only reinforcement, or in combination with traditional steel rebars.

Many factors affect the mechanical performance of SFRC: fiber type and amount, casting method and compressive strength, but one key aspect of SFRC which was, and still is, strongly analyzed and debated is fiber orientation [2, 10, 11]. In fact, fibers perpendicular to the crack plane contribute to the residual tensile strength by bridging cracks [12] while fibers parallel to the crack plane have little efficiency. Fiber orientation could be a problem for a SFRC structure but, if well managed, may become an opportunity for enhancing SFRC performances. A thorough review on the topic and the methods to assess it is drawn by Alberti et al. [13], discussing the parameters affecting it and their influence on the mechanical performance of the structural element.

An ideal solution for structural elements would be to force fiber orientation into the most advantageous direction to optimize the performance of this anisotropic material [1]. Of paramount importance to fiber orientation are border effects [10, 11, 14–17] and the flow regime of concrete during casting [12, 18–20]. Some research studies attempted to force the fiber orientation either by taking advantage of the aforementioned border and flow effects [21, 22], or by magnetism [23, 24]. The experimental results were, for the former, dependent on formwork size and shape and, for the latter, obtained on small specimens, using ad-hoc mortars.

In the present research study, a new casting method is developed to force fibers into an almost one-directional orientation by exploiting vibration and using a series of narrow channels, independent of formwork size and shape.

It should be also observed that, among researchers and practitioners, a major concern is raising about the representativeness of EN 14651 [25] beams for measuring the mechanical properties of SFRC for structural design [26–28]. In fact, such beams could have a better overall post-cracking performance than SFRC in a real structure, due to a more favorable fiber orientation along the main direction of the beam, thus perpendicular to the crack starting from the notch, because of their geometry and the casting procedure [29, 30]. For this reason, structural codes refer to effective mechanical properties that take into account orientation factors [5]. As such, many methods are known in literature to assess fiber orientation in SFRC [13, 18, 31, 32], in order to relate it to the effective residual tensile properties provided by SFRC in the real element. They can be direct or indirect, destructive or not. Two of these methods have been adopted in this research, for the first time on a hybrid system of macro and micro fibers, in order to compare the post-cracking mechanical properties of specimens which only differ in fiber orientation.

2 Experimental program and method

2.1 Material and mix design

The concrete material chosen for the experimental campaign is a high performance concrete (HPC) with a water/cement ratio of 0.46, reinforced with 120 kg/m^3 of macro and micro fibers, dosed in equal amount (60 + 60 kg/m^3) [32, 33]. Table 1 summarizes the main characteristics of the three fiber types adopted (two macro and one micro fibers). The SFRC mix is kept constant for all specimens, except for the type of macro fiber and the amount of superplasticizer, which differentiate SFRC specimens into two series; the 60_Series has 60 mm long, triple-hooked end macro fibers, while the 35_Series has 35 mm long, single-hooked end macro fibers. The superplasticizer was dosed to obtain similar workability between the two series. A retarder was also included in the mix to grant longer workability of the fresh concrete, needed for this new casting methodology. The mix design characteristics of the two series are shown in Table 2. All concrete batches were obtained by firstly mixing the dry components in a 250 L pan mixer for 45 s, then adding water and superplasticizer and mixing for 150 s, and finally adding steel fibers and retarder and mixing for 90 s.

2.2 Description of the orientation device

The device to impose a one-dimensional orientation to the fibers was designed and produced at the Ruhr University Bochum, and exploits the thixotropy of concrete, which is the property of becoming less viscous when subjected to an applied stress, for example vibration. After mixing, the material is cast in a container on top of the orientation device; by

Table 1 Characteristics of the steel fibers

Fiber designation	Dramix 5D 65/60 BG	Dramix 3D 65/35 BG	Dramix OL 13/0.20
Shape	Triple-hooked end	Single-hooked end	Straight
Length, l (mm)	60	35	13
Diameter, ∅ (mm)	0.90	0.55	0.20
Aspect ratio, l/∅	65	65	65
Tensile strength (MPa)	2300	1345	2750
Elastic modulus (GPa)	200	200	200

Table 2 Constituents of the SFRC mixture

Material designation	60_Series	35_Series
Cement CEM I 52.5 R (kg/m^3)	450	450
Fly ash (kg/m^3)	100	100
Quartz sand 0.063–0.25 mm (kg/m^3)	100	100
Sand 0–2 mm (kg/m^3)	850	850
Gravel 2–8 mm (kg/m^3)	565	565
Water (kg/m^3)	205	205
Retarder BASF MasterSet R 436 (% of cement content)	0.3	0.3
Superplasticizer BASF Glenium ACE 480 (% of cement content)	0.35	0.3
Macro steel fiber type	Dramix 5D 65/60 BG	Dramix 3D 65/35 BG
Macro steel fiber content (kg/m^3)	60	60
Micro steel fiber type	Dramix OL 13/0.20	Dramix OL 13/0.20
Micro steel fiber content (kg/m^3)	60	60

opening the container, concrete falls on a series of narrow U-shaped channels (cf. Figure 1a). The workability of the fresh composite is intentionally poor, between 40 and 50 cm in flow table test [34] so that, without vibration, concrete remains above the channels and does not flow along them. Two external vibrators are fixed to the device and impose a vibration to the channels and, in turn, to the concrete. By effect of such vibration, concrete starts settling into the channels and flowing along them. Due to their narrowness and length, flow and border effects act on the concrete, causing fibers to align in flow direction [12, 19]. At the end of the channels, concrete settles at one end of a large formwork (cf. Figure 1b), which is free of any vibration. As vibration stops, the material loses any flowability and remains in place with the fibers one-dimensionally oriented. As concrete keeps flowing down the device and into the formwork, the latter is pulled back accordingly, so that a homogeneous strip of concrete, of about 50 mm height, is cast. Due to the low workability of the fresh mixture, the strip of concrete in the formwork does not need to be in contact with the vertical wooden borders, but keeps its shape independently. This allows for the casting of multiple strips one next to the other, and also on top of each other, until the formwork is completely filled with concrete. At this point, the formwork is vibrated for about 5 s on a vibrating table to ensure perfect homogenization between the strips, both vertically and horizontally, and a smooth top surface. An optimization of design parameters of the device was priorly carried out to define an optimal length, width and inclination of the channels; for further information on the optimization process, refer to [35].

2.3 Specimens description

In the present experimental campaign, the orienting device set the concrete into 150 mm deep, 610 × 610 [mm] formworks. Since the device is 300 mm wide,

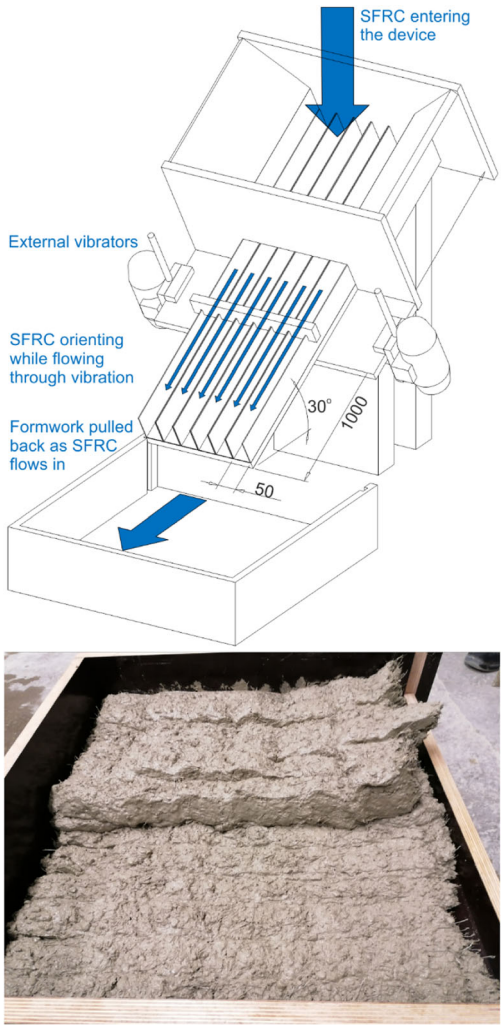

Fig. 1 **a** Schematic representation of the orienting device and its functioning (measures in mm); **b** intermediate result of the casting procedure using such device (SFRC strips are clearly visible)

and sets 50 mm deep strips of concrete, two sets of strips were cast next to each other, on three vertical layers, to completely fill the formwork. This ensured that each plate could be cut into three standard beams 150 × 150 × 610 [mm] to perform a 3-point bending test according to EN 14651 [25]. The two sides of the plate in contact with the formwork, in the longitudinal direction of the cut beams, were discarded for a width of 80 mm on each side, to avoid the zones affected by border effects [15, 27]. Depending on the direction of the cut, either parallel or perpendicular to the casting direction, beams with a favorable or unfavorable fiber orientation were produced, respectively (cf. Figure 2). In fact, during a 3-point bending test, fibers oriented along the longitudinal axis of the beam (and, consequently, perpendicular to the crack plane), have a favorable effect on the residual tensile strength of the element [12, 29]; such specimens will be referred to as "well oriented (W)". On the other hand, fibers oriented parallel to the crack plane provide a minor contribution to the residual strength properties of SFRC [28]; such beams will be called "badly oriented (B)".

For the sake of comparison, additional plates with dimensions 150 × 610 × 610 [mm] were cast in a traditional way; concrete was poured from a large container, with outlet diameter of 300 mm, positioned centrically on top of the plate, and then compacted by external vibration. Due to the low workability of the fresh mixture, the fiber orientation of these specimens was considered roughly isotropic [12], even though one can expect a tendency towards a two-dimensional planar orientation [36, 37]. The plates were then cut with the same procedure of the oriented specimens, and three beams free from external border effects were obtained from each plate. These specimens will be referred to as "isotropic (I)".

Finally, some beams were cast according to EN 14651 [25], in 150 × 150 × 700 [mm] steel formworks. Fibers in beams produced in compliance with such norm will be subject to border effects [26, 27, 29], but not as strongly as the ones steered with the orienting device. Such beams will be called "standard (S)".

For each concrete batch, either two plates or six standard beams were cast, together with three cubes of 150 mm edge length for determining the compressive strength ($f_{cm,cube}$).

In the 60_Series (with 60 mm long macro fibers), each batch of concrete was used to cast one specific series, which means that the first batch was used to cast the well oriented specimens (60_W), the second to produce beams according to EN 14651 (60_S), the third to cast isotropic elements (60_I) and the fourth to make badly oriented specimens (60_B).

In the 35_Series, instead, each batch was used to produce plates having different fiber orientations. In fact, the first concrete batch of the series (batch 5) was used to cast one well oriented plate and an isotropic plate. The second batch (batch 6) was used for one badly oriented and an isotropic plate, while the third one (batch 7) was used for a well oriented and a badly

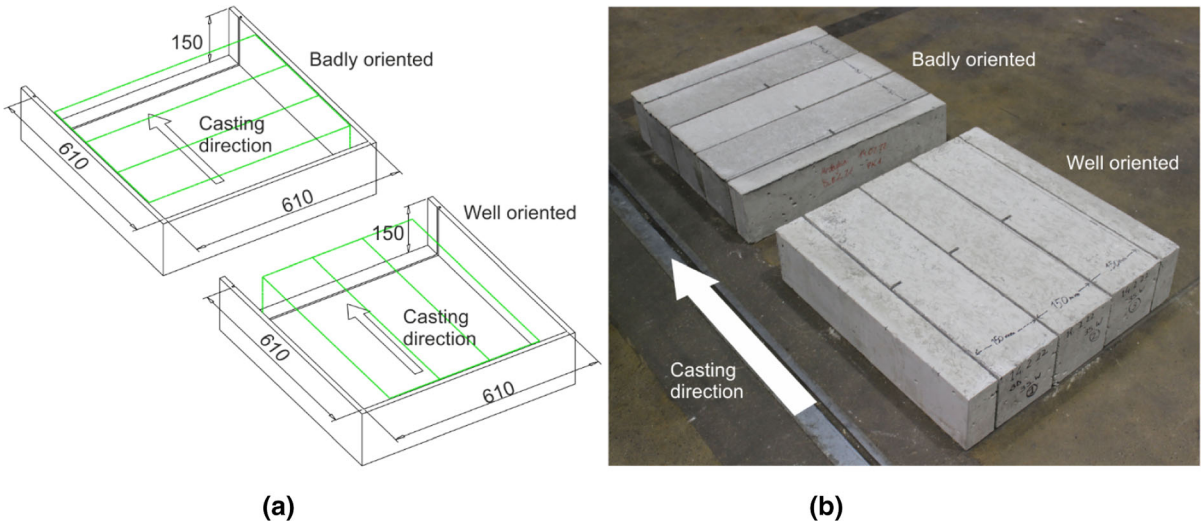

Fig. 2 **a** Schematic and **b** photographic representation of the well and badly oriented specimens produced with the orienting device

Table 3 Performance of concrete in the fresh and hardened state

Series designation	60_Series				35_Series						
	60_W	60_S	60_I	60_B	35_W 1	35_W 2	35_S	35_I 1	35_I 2	35_B 1	35_B 2
Batch number	1	2	3	4	5	7	8	5	6	6	7
Flow table test (cm) [34]	46	53	46	40	44	41	50	44	58	58	41
$f_{cm,cube}$ (MPa)	79.3	79.0	79.3	76.9	79.8	68.1	62.3	79.8	68.1	68.1	68.1

oriented plate. The standard beams were lastly produced in a single cast (batch 8). This approach was chosen to check the repeatability of the method as well as to directly compare specimens having different fiber orientation made of concrete belonging to the same batch; in this manner, fiber orientation was the only parameter being varied. Indeed, many factors affect the residual tensile strength of concrete. Besides border effect, fiber length, aspect ratio and amount, also workability of the fresh mixture, compaction and compressive strength of the hardened concrete play a significant role [16, 38, 39]. The authors have taken care to keep these parameters constant, but small differences between batches are expected.

The aim of the concrete mix design was to achieve a mean cubic compressive strength of 80 MPa after 28 days of curing in a climatic chamber at 20 °C, and a flow table test spread between 40 and 50 cm [34]; this goal was achieved for all batches of the 60_Series, while some batches of the 35_Series deviated from it having a lower compressive strength (cf. Table 3).

3 Experimental results and discussion

Six beams were tested for each series. Each beam was firstly subjected to mechanical testing in a 3-point bending set-up according to EN 14651 [25] to measure the residual flexural tensile strength. The testing machine was operating in a controlled manner, producing a constant rate of deflection in the beams. Afterwards, a cube (150 mm side) was saw cut from each beam at a distance of 30 mm from the central notch, to measure orientation of fibers (inside the cube) by using an indirect electromagnetic induction method, called “BSM100” [40]. Finally, to verify the results of the orientation measuring method, one cubic sample of 35 mm side was extracted from an untested beam for each configuration of the 35_Series (W, S, I

and B) and analyzed with micro computed tomography. This sample was saw cut in the middle of the longitudinal length of the beam, and in the center of the cross section.

3.1 Mechanical properties of the hardened specimens

The experimental results of the bending tests are shown in Fig. 3 in terms of nominal stress versus vertical displacement. Table 4 summarizes the residual flexural tensile strength parameters according to the *fib* Model Code 2010 [5], and the comparison, in terms of a ratio, of f_{R1} and f_{R3} (which represent the post-cracking strength at serviceability and ultimate limit states, respectively [5]) measured for each fiber orientation with respect to the standard casting method according to EN 14651 [25].

The analysis of results for the 60_Series is straightforward. Since the compressive strength of all batches is very similar, one can directly compare the curves and observe that each batch has a distinct behavior and reaches different bending tensile stress levels. The only similarity is between 60_W and 60_S specimens, which have a comparable performance during the first part of the test and a small difference for larger crack openings (with f_{R3} 9% larger in 60_W specimens). This clearly shows how the standard casting method produces a favorable fiber orientation in the beams, especially for 60 mm long fibers. 60_B elements, as expected, show the worst performance, about 60% lower than 60_S while 60_I specimens fall in between 60_B and 60_S. The coefficients of variation are rather modest, varying between 3 and 14%; the lower values belong to 60_W series, which shows high performances and very low scatter of results, while 60_I series exhibits the highest coefficient of variation, due to the randomness in orientation of fibers during casting, which is not driven by any steering effect.

The analysis of results for the 35_Series, on the other hand, cannot be performed on this scale. The compressive strength of the different batches ranges between 62 and 80 MPa, thus making the comparison of nominal stress less significant. For this reason, Fig. 4 presents the curves of the 35_Series normalizing the stress on the basis of the tensile strength, assumed proportional to the square root of $f_{cm,cube}$ (as already done by [39]). Table 5 summarizes the normalized residual flexural tensile strength parameters and, again, the comparison with standard elements.

In Fig. 4 the elements belonging to the same casting method (W, S, I or B), but cast in different batches,

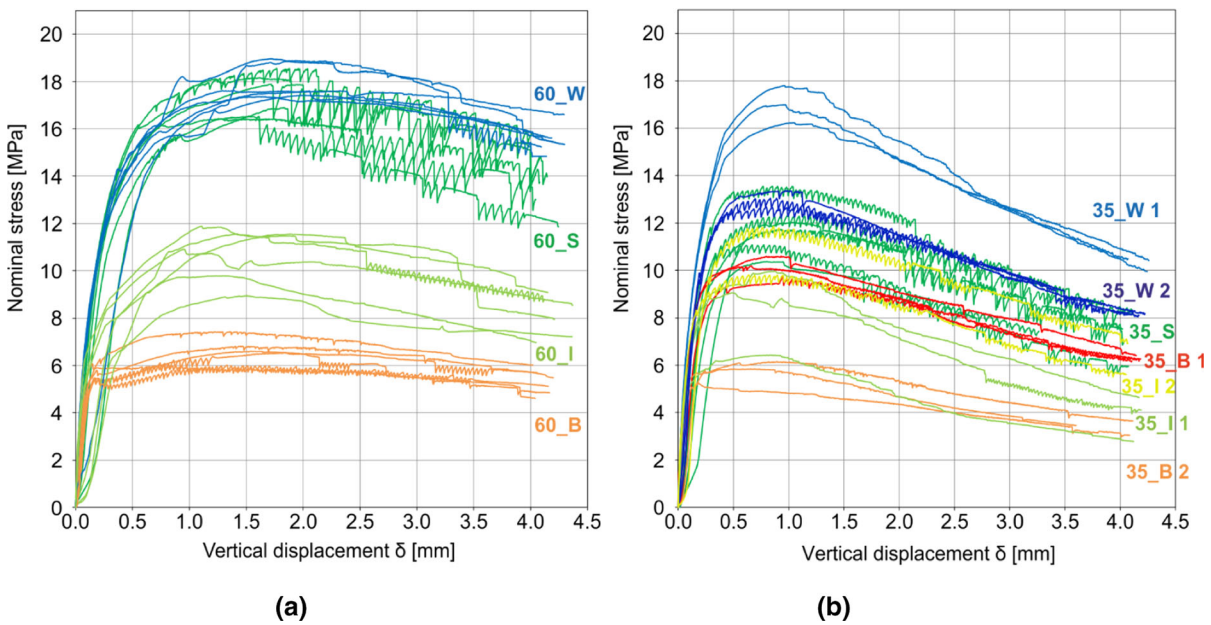

Fig. 3 **a** Nominal stress versus vertical displacement curves of the 60_Series and **b** of the 35_Series

Table 4 Mean residual flexural tensile strength values and comparison to the standard beams

	$f_{R1,m}$ [MPa]	$f_{R2,m}$ [MPa]	$f_{R3,m}$ [MPa]	$f_{R4,m}$ [MPa]	$f_{R1,m}/f_{R1,m,S}$ [–]	$f_{R3,m}/f_{R3,m,S}$ [–]
60_W (CV)	13.96 (0.09)	17.35 (0.03)	17.82 (0.04)	17.35 (0.03)	0.99	1.09
60_S (CV)	14.10 (0.10)	17.05 (0.05)	16.40 (0.06)	15.64 (0.08)	–	–
60_I (CV)	8.38 (0.13)	10.54 (0.11)	10.20 (0.13)	9.48 (0.14)	0.59	0.62
60_B (CV)	5.87 (0.09)	6.47 (0.09)	6.33 (0.08)	5.97 (0.09)	0.42	0.39
35_W 1 (CV)	15.56 (0.04)	16.64 (0.05)	14.52 (0.03)	12.55 (0.01)	1.42	1.47
35_W 2 (CV)	12.55 (0.02)	12.49 (0.02)	11.12 (0.02)	9.77 (0.01)	1.15	1.13
35_S (CV)	10.94 (0.11)	11.37 (0.10)	9.85 (0.09)	8.49 (0.10)	–	–
35_I 1 (CV)	8.20 (0.21)	7.75 (0.23)	6.21 (0.24)	4.97 (0.27)	0.75	0.63
35_I 2 (CV)	10.34 (0.10)	10.35 (0.14)	9.21 (0.16)	7.84 (0.18)	0.95	0.93
35_B 1 (CV)	9.78 (0.05)	9.66 (0.03)	8.62 (0.03)	7.55 (0.04)	0.89	0.87
35_B 2 (CV)	5.60 (0.10)	5.30 (0.11)	4.59 (0.10)	3.97 (0.09)	0.51	0.47

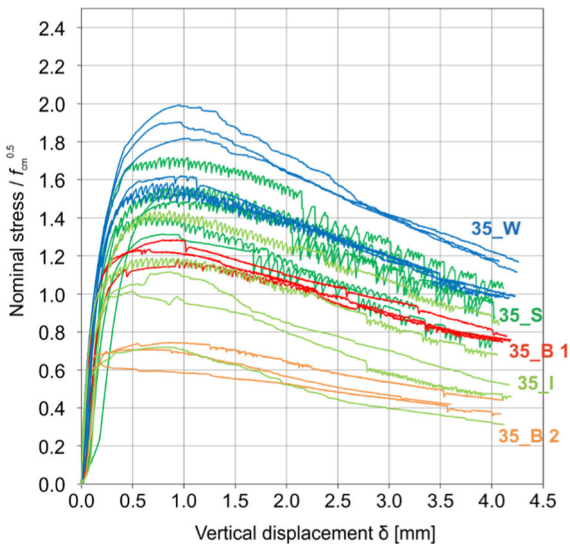

Fig. 4 35_Series: experimental results of the nominal stress normalized to the square root of $f_{cm,cube}$

were grouped together when a sufficiently similar performance was noted. This is the case for 35_W 1 and 35_W 2 specimens, where the latter batch shows a slightly lower overall performance, but still above all other batches on average. These curves were all grouped under the 35_W label. This homogenization is instead not possible with 35_B 1 and 35_B 2 batches since the workability of the former was significantly above the limit chosen during casting (cf. Table 3) and the casting method was partially ineffective. In fact, after concrete left the orienting device and was set into the formwork, a certain degree of flowability (in absence of vibration) was registered, causing a partial loss of fiber orientation. The performance of batch 35_B 1 is hence closer to a two-dimensional fiber orientation, and its performance is between isotropic and standard; thus, these specimens cannot be regarded as badly oriented. The second part of such batch was used to cast 35_I 2 plate but this casting technique is less susceptible to workability variations. A more fluid concrete would mean an orientation closer to two-dimensional, rather than isotropic, because of a higher impact of vibration [12], but the absence of nearby formwork borders means that fibers will still be randomly oriented, at least in the horizontal plane. For this reason, batches 35_I 1 and 35_I 2 can be treated like 35_W. The latter tends to be closer to 35_S values, while the former behaves closer to 35_B elements (cf. Figure 3b), but still in sufficient consistency, considering the intrinsic high scatter possible with this kind of casting method. All curves were grouped under the 35_I label. 35_B 2 elements actually show the performance of badly oriented fibers; the workability of the batch was within the limits, and the residual bending tensile strength is about 50–55% lower than 35_S. Finally, it can be observed that 35_W beams show an average increase in performance of almost 20% with respect to 35_S (cf. Figure 5b).

Figure 5 shows the average curves for 60_Series and 35_Series, and the relative difference in performance with respect to the elements cast with the standard method of EN 14651 [25].

Table 5 Mean residual flexural tensile strength values homogenized to the square root of $f_{cm,cube}$ and comparison to the standard beams

	$f_{R1,m}/(f_{cm})^{0,5}$ [–]	$f_{R2,m}/(f_{cm})^{0,5}$ [–]	$f_{R3,m}/(f_{cm})^{0,5}$ [–]	$f_{R4,m}/(f_{cm})^{0,5}$ [–]	$\frac{f_{R1,m}/(f_{cm})^{0.5}}{f_{R1,m,35\_S}/(f_{cm,35\_S})^{0.5}}$	$\frac{f_{R3,m}/(f_{cm})^{0,5}}{f_{R3,m,35\_S}/(f_{cm,35\_S})^{0.5}}$
35_W (CV)	1.63 (0.08)	1.69 (0.12)	1.49 (0.10)	1.29 (0.09)	1.18	1.19
35_S (CV)	1.39 (0.11)	1.44 (0.10)	1.25 (0.09)	1.08 (0.10)	–	–
35_I (CV)	1.05 (0.23)	1.02 (0.26)	0.86 (0.32)	0.71 (0.36)	0.76	0.69
35_B 1 (CV)	1.18 (0.05)	1.17 (0.03)	1.04 (0.03)	0.91 (0.04)	0.86	0.84
35_B 2 (CV)	0.68 (0.10)	0.64 (0.11)	0.56 (0.10)	0.48 (0.09)	0.49	0.45

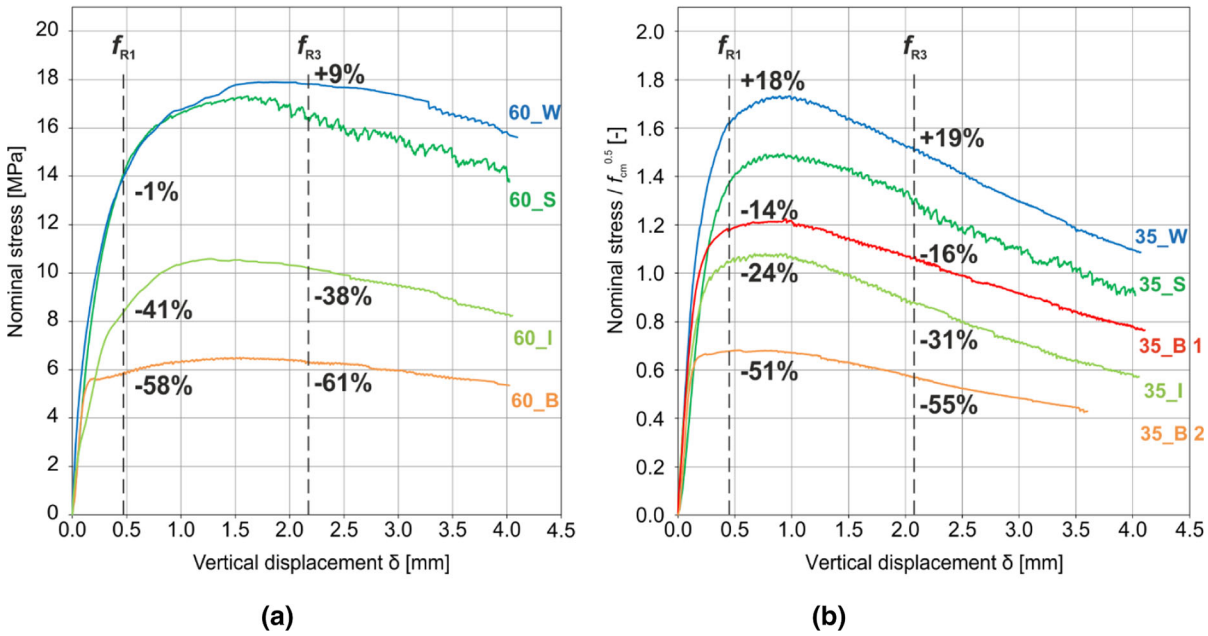

Fig. 5 **a** Nominal stress versus vertical displacement mean curves of the 60_Series; **b** normalized nominal stress versus vertical displacement mean curves of the 35_Series; the percentages refer to the results from the standard beams

All specimens show an immediate hardening response after first cracking, even the ones with badly oriented fibers. This is due to the high fiber amount chosen, and to the presence of micro fibers, very effective in bridging micro cracks.

Generally, the casting method according to EN 14651 [25] allows a rather good fiber orientation to the specimens, lower only than a strong one-dimensional fiber orientation obtained with a dedicated device. This trend is particularly evident for longer macro fibers (cf. Figure 5a), where 60_W elements have a rather small increase in performance with respect to 60_S. On the other hand, for shorter macro fibers (35_Series) this increase is more than doubled. This is due to a larger influence of the border effect in 60_S specimens, since it is proportional to the fiber length [11, 15]. As expected, the orientation along the longitudinal axis of the standard beams is more pronounced than the one found in the isotropic situation [26, 27, 29].

Interestingly, well oriented specimens have a residual tensile strength about three times higher than badly oriented ones, using the same casting technique and varying only the direction in which the beams were cut from the plates, with respect to the casting direction (cf. Figure 3). This is an indication of the

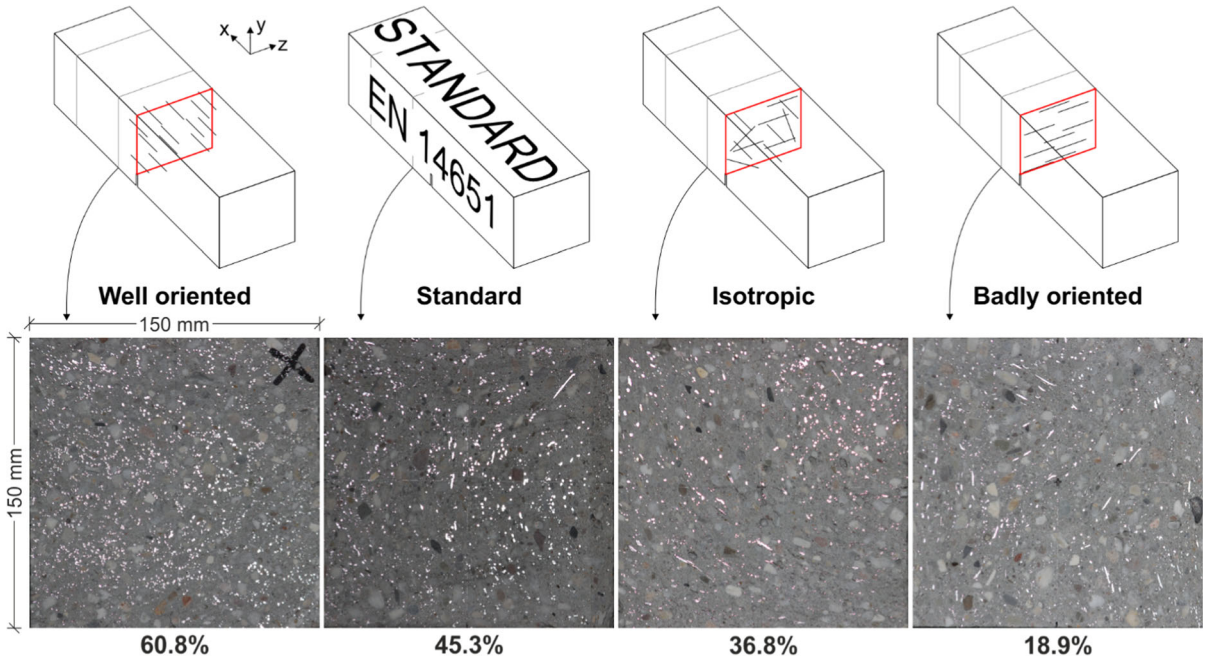

Fig. 6 Schematic representation of fiber orientation on the crack surface for each specimen type (top), and cut cross-sections at 30 mm from the notch, with fibers visible thanks to the camera flash (bottom). Below, the average fiber orientation measured with BSM100 in the *X* direction for the 35_Series is displayed

soundness of the orienting device, and of the high impact of fiber orientation on the mechanical performance of a structural element.

The orienting method tested and presented in this research proved to be susceptible to changes in concrete workability. In particular, a fluid concrete reduces the efficiency of the orientation device. On the other hand, the device proved robust in the range of fiber lengths that can be oriented. Both 35 and 60 mm fibers were effectively oriented in one direction.

3.2 Methods for assessing fiber orientation

After mechanical testing, the beams were cut orthogonal to the longitudinal direction to obtain cubes with 150 mm side. The cubes were taken at 30 mm from the central notch, as close as possible to the beam's central section for representativeness of the crack surface, but far enough not to cross the crack itself.

It should be observed that the fibers visible on the cross-sectional cuts differed significantly between the series. In fact, well oriented specimens show a high number of fibers on the cross-section, all with a shape close to a circle (because perpendicular to the crack surface). Badly oriented specimens display far fewer fibers, and with elongated (elliptical) shapes. Standard and isotropic elements exhibit an intermediate trend, with the standard closer to well oriented beams, and the isotropic leaning towards the badly oriented. This tendency is well known in literature and supported by theory [2, 15, 39]. Figure 6 shows on top the schematic fiber orientation expected at the central section for each series, and below the photograph of the cross-section closer to the notch after cutting a generic beam for each series. Underneath, the average amount of fibers oriented along the longitudinal axis (perpendicular to the cross section) of the beam of the 35_Series is reported; such value was measured with the electromagnetic induction method on the cubes extracted from the beams, as is described in detail in Sect. 3.2.1.

Besides the qualitative considerations that can be made from observation of cross section cuts, two methods were employed to quantitatively determine fiber orientation in the beams for the different casting techniques. The first is an indirect electromagnetic induction method, which measures the average fiber orientation in a 150 mm cube along the three principal directions. The second is micro-computed tomography, a direct method to exactly reconstruct the position

Table 6 Mean values obtained from the BSM100, in terms of percentage of fibers oriented in each direction. Bold values will be compared with computed tomography results in Section 3.2.2

Series designation	60_Series				35_Series				
	60_W	60_S	60_I	60_B	35_W	35_S	35_I	35_B 1	35_B 2
Orient. in **X** (%) (CV)	56.88	56.22	41.90	26.82	**60.82**	**45.33**	**36.82**	29.43	**18.93**
	(0.04)	(0.02)	(0.07)	(0.10)	(0.06)	(0.12)	(0.18)	(0.25)	(0.05)
Orient. in **Y** (%)	28.62	26.68	42.45	57.05	**24.20**	**31.87**	**41.64**	47.40	**60.23**
(CV)	(0.11)	(0.13)	(0.05)	(0.03)	(0.18)	(0.10)	(0.10)	(0.07)	(0.02)
Orient. in **Z** (%)	14.52	17.07	15.67	16.15	**15.00**	**22.77**	**21.56**	23.17	**20.83**
(CV)	(0.10)	(0.15)	(0.18)	(0.13)	(0.11)	(0.18)	(0.29)	(0.20)	(0.08)

of fibers inside a cube of 35 mm edge length. The former was applied to all cubes extracted from the mechanically tested beams; the latter was performed on a total of four cubes, one for each kind of the 35_Series, as a control measure of the soundness of the ferromagnetic induction values.

3.2.1 Electromagnetic induction results

The use of an electromagnetic induction method to measure fiber orientation in concrete samples has been widely used in literature [13, 41]. The steel fiber measuring device used in this study is known as "BSM 100", and is based on an induction measurement system where a cubic concrete sample is positioned in a coiled sensor and exposed to an alternating magnetic field. By measuring the induction voltage obtained through the sample, the average value of fiber orientation along the three principal directions can be obtained. Further details on the method can be found in [32, 40].

The dependence of the induction voltage U_i on the angle α between the steel fibers and the magnetic field was defined experimentally [40], and can be described as follows:

$$U_i = U_{i,\max} \cdot (1 - \sin \alpha) \quad (1)$$

The induction voltage in the induction coil is maximum ($U_{i,\max}$) when all steel fibers are aligned along the field lines, while it is negligible when fibers are perpendicular to the field direction. Consequently, by measuring the induction voltage U_i in the three spatial directions, the average fiber orientation along each of them can be extrapolated. If the induction is greater in one spatial direction, proportionally more fibers [according to Eq. (1)] are oriented along it than in the other two spatial directions. A significant advantage of this method is that the fiber orientation of the sample can be determined independently from fiber type and without prior calibration. The outcome is in the form of three percentages, one for each principal direction, with the values adding up to 100% and representing the relative theoretical amount of fibers oriented along each direction.

The result of fiber orientation in each of the three principal directions is given in Table 6. In particular, *X* is the longitudinal direction of the beams, that is perpendicular to the crack plane in the 3-point bending test. *Y* is the other planar direction, parallel to the ground during casting, while *Z* is the vertical direction during casting.

As already mentioned, fibers oriented perpendicular to the crack plane are able to bridge the cracks and improve the residual tensile strength of a concrete element, while fibers oriented parallel to the crack plane do not contribute to the post-cracking tensile strength [36, 42]. For this reason, the orientation values along the *X* direction can be linked to the mechanical performance of the beams. Such values monotonically increase with the same trend of the residual flexural tensile strength values reported in Tables 4 and 5, with the worst performance recorded for the badly oriented fibers, followed by the isotropic, then by the standard, and lastly by the well oriented fibers. It can be observed that in specimens made with the proposed setup, the fiber orientations in the two planar directions during casting, *X* and *Y*, are inverted in beams cut (from the plate) along or perpendicularly to the casting direction. The fiber orientation percentages are also very similar between 60 and 35_Series, especially in beams made with the proposed setup; this is a further demonstration of the effectiveness of the

orienting device. On the other hand, in standard beams the orientation percentage is higher in elements with longer fibers, due to the higher influence of wall effects.

The mean orientation value along X of 60_S is considerably high, and almost identical to that of 60_W. This proves the favorable fiber orientation imposed by the standard EN 14651 [25] casting method, especially for 60 mm long fibers, which generates specimens with an orientation close to mono-dimensional. This is also coherent with the residual tensile strength showed by 60_S and 60_W specimens in the 3-point bending tests, which is comparable up to a vertical deformation of 1 mm, and deviates by 9% at f_{R3}.

A similar trend can be observed for 35_S elements, with the X direction being the predominant orientation, but the fiber orientation percentage is lower than in 35_W elements and is closer to 35_I specimens. Once again, this can be linked to the fact that shorter fibers are less susceptible to border effects generated in the 150 mm wide standard formwork. The homogenized residual bending tensile strength of 35_S beams follows the same trend, and is almost 20% lower than 35_W elements.

The mean orientation along Z, corresponding to the vertical direction during casting, is in general the lowest value among the three principal directions. This is coherent with the fact that, during the casting process, fibers tend to orient in horizontal planes, perpendicular to gravity [14, 36, 37]. For this reason, specimens cast with the isotropic method do not show a homogeneous three dimensional fiber orientation, but rather tend to a two-dimensional distribution.

The observations made about batch 35_B 1 are supported by fiber orientation results. The Y axis is the principal orientation direction (47%), but the value is well below that of batch 35_B 2, and is more similar to the impact of border effects on standard specimens along the X axis (45%). Therefore, the casting procedure had a remarkable effect on orienting the fibers but its steering effect was reduced by the higher workability of the SFRC mix. Furthermore, the fiber orientation percentage along the X axis, which affects the mechanical performance of the beam, has the highest scatter. However, the mean normalized residual tensile strength of 35_B 1 is higher than that of 35_I, even though the fiber orientation percentage is higher in 35_I specimens. A factor that may cause such discrepancy in the correlation between residual tensile parameters and fiber orientation is that the former depends on the amount and orientation of fibers crossing the crack, while the latter is calculated as an average on a volume close to the crack.

Figure 7 represents the correlation between the mean fiber orientation along the X axis (obtained with the electromagnetic induction method) and the residual flexural tensile strength values (obtained in the 3-point bending tests), for both 60_Series and 35_Series. The two variables were linked via a linear regression model and its accuracy was evaluated by means of the coefficient of determination (R^2). Both regressions of the 60_Series show high accuracy (R^2 = 0.86 and 0.93 for f_{R1} and f_{R3}, respectively), while the 35_Series have lower coefficients of determination (R^2 = 0.75 and 0.73 for f_{R1} and f_{R3}, respectively). The latter is due to some points which deviate pronouncedly from the trend line, two of which belong to the 35_B 1 batch. Despite the previous considerations, such batch was not excluded from the model, since the workability of the fresh mixture certainly influences fiber orientation, but should not affect significantly the relation between fiber orientation and residual tensile strength. In fact, the isotropic specimens 35_I 2, cast with the same batch of 35_B 1, lay very close to the trend line. However, as mentioned above, the post-cracking mechanical properties are strongly influenced by fiber orientation and fiber density at the crack surface, while the fiber orientation percentages were determined on a volume next to it.

A 95% confidence interval about the regression line was also constructed, as it is shown on the graphs (black long-dotted line); the width of these confidence intervals is a measure of the overall quality of the regression. Another statistical parameter defined in the graph is the 95% prediction interval on a future observation (grey short-dotted line); it provides an interval estimate of the dependent variable (f_{R1} or f_{R3}) from a future observation of orientation along the X axis of specimens with the same characteristics as those tested in the present experimental campaign. For example, for a beam of the 60_Series with measured orientation along the X axis of 40%, the 95% estimate of mechanical performance would be between 6 and 12 MPa for f_{R1}, and between 8 and 13.5 MPa for f_{R3}. If the confidence intervals appear narrow, and provide an indication of good coherence of the data, the prediction intervals are wide and, especially for the

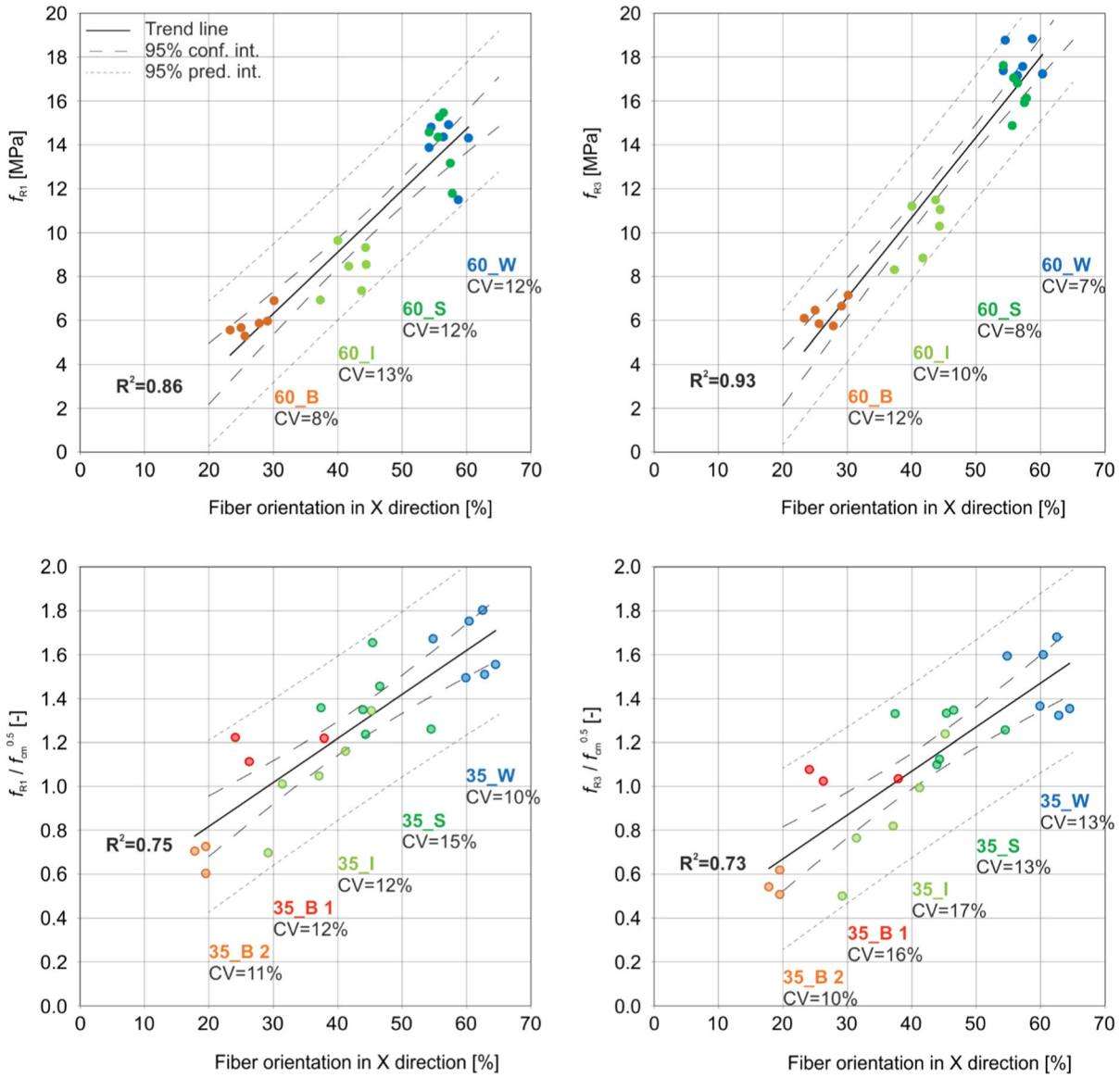

Fig. 7 Correlation between residual flexural tensile strength values and fiber orientation in *X* direction obtained with BSM100

35_Series, do not allow for an adequate estimation of future measurements. More experimental tests on the same series would reduce the interval width and provide better predictions.

Table 7 summarizes, for all series, mean values of orientation along the *X* direction and residual tensile strength parameters. For the latter, standard deviation (σ) and coefficient of variation (CV) of each series from the linear trend is reported. An overall low CV can be seen among the series. Regarding f_{R3} values of the 60_Series, an increase in performance determines a decrease in the CV. The same can be stated for the homogenized f_{R3} values of the 35_Series, when the two 35_B batches are grouped together. In this way, the coefficient of variation of the global 35_B series becomes 23%.

3.2.2 *Micro-computed tomography results*

Industrial micro computed tomography (CT) is an X-ray based non-destructive 3D measurement technique which is capable of visualizing the internal and

Table 7 Mean values obtained from the BSM100 in *X* direction and mean residual flexural tensile strength values. Standard deviation and coefficient of variation of the latter from the linear trend are also reported

Series designation	60_Series				35_Series				
	60_W	60_S	60_I	60_B	35_W	35_S	35_I	35_B 1	35_B 2
Orient. In X (%)	56.88	56.22	41.90	26.82	60.82	45.33	36.82	29.43	18.93
f_{R1} (MPa)	13.96	14.10	8.38	5.87					
σ (MPa)	1.62	1.67	1.09	0.45					
CV (%)	11.6	11.9	13.1	7.6					
f_{R3} (MPa)	17.82	16.40	10.20	6.33					
σ (MPa)	1.22	1.25	1.06	0.78					
CV (%)	6.8	7.6	10.4	12.3					
$f_{R1.m}/(f_{cm})^{0.5}$ (–)					1.63	1.39	1.05	1.18	0.68
σ (–)					0.16	0.20	0.12	0.14	0.07
CV (%)					9.7	14.5	11.8	11.8	11.0
$f_{R3.m}/(f_{cm})^{0.5}$ (–)					1.49	1.25	0.86	1.04	0.56
σ (–)					0.19	0.16	0.15	0.16	0.06
CV (%)					13.0	12.8	17.5	15.6	9.95

external features of the sample simultaneously. Although the concept originates from the medical field, over the last decade, advancement in hardware and software domain has paved its way to becoming a highly precise industrial tool not only for qualitative imaging but also for quantitative 3D analysis of, for example, porosity [43, 44], crack detection [44], dimensional measurements [45] and multi-material segmentation [46].

The resolution of CT scans was set to 20 µm, ten times smaller than the diameter of the micro fibers. This high resolution allows to even accurately measure and depict the hooked end of macro fibers. The samples were scanned with an X-ray voltage of 220 kV with 10 W and 4500 projections were captured on a detector with 3200 × 2304 pixels with a pitch of 120 µm. The exposure time was 2.8 s. The volume was reconstructed using filtered back projection. Subsequently, a median filter with a window of 5 was applied to it. This volume was then thresholded to create a Region of Interest (ROI) for the fibers and a region refinement was performed afterwards to accurately obtain the fiber edges. This ROI was then analyzed with VGSTUDIOMAX 3.5 for fiber orientation analyses. Differently from the electromagnetic induction method, from the CT scans, the fiber volume fraction and the orientation of each individual fiber can be extracted. Further details can be found in [47].

Fiber orientation inside the volume can be computed as:

$$O_{(\text{axis})} = \frac{1}{n}\sum_{i=1}^{n} \cos^2 \vartheta_{\text{axis}} \tag{2}$$

where $O_{(\text{axis})}$ is the orientation along one of the three principal axes, n is the total number of fibers found in the volume, ϑ_{axis} is the angle between the fiber and the principal axis involved.

This method of calculating fiber orientation diverges from the more renowned and widespread formulas first adopted by Soroushian and Lee [2] and by Schönlin [48], which consider the orientation of fibers found on a two-dimensional surface. Each $O_{(\text{axis})}$ is, in fact, a diagonal component of the orientation tensor describing the three dimensional fiber configuration inside a concrete volume [26, 49]. The advantage of this formulation is that fiber orientation values in the three directions obtained in this way add up to 1, thus seeming particularly suited for expressing and comparing the orientation state in a volume. Moreover, such values can be expressed in percentage form, to be directly compared to the BSM100 results.

Such comparison shows good agreement, as can it be seen by analyzing the CT results presented in Fig. 8c and the bold values from BSM100 in Table 6. For both measuring methods, the trend of orientation in the different series is similar, with a discrepancy of less than 10% for all values. The highest value along

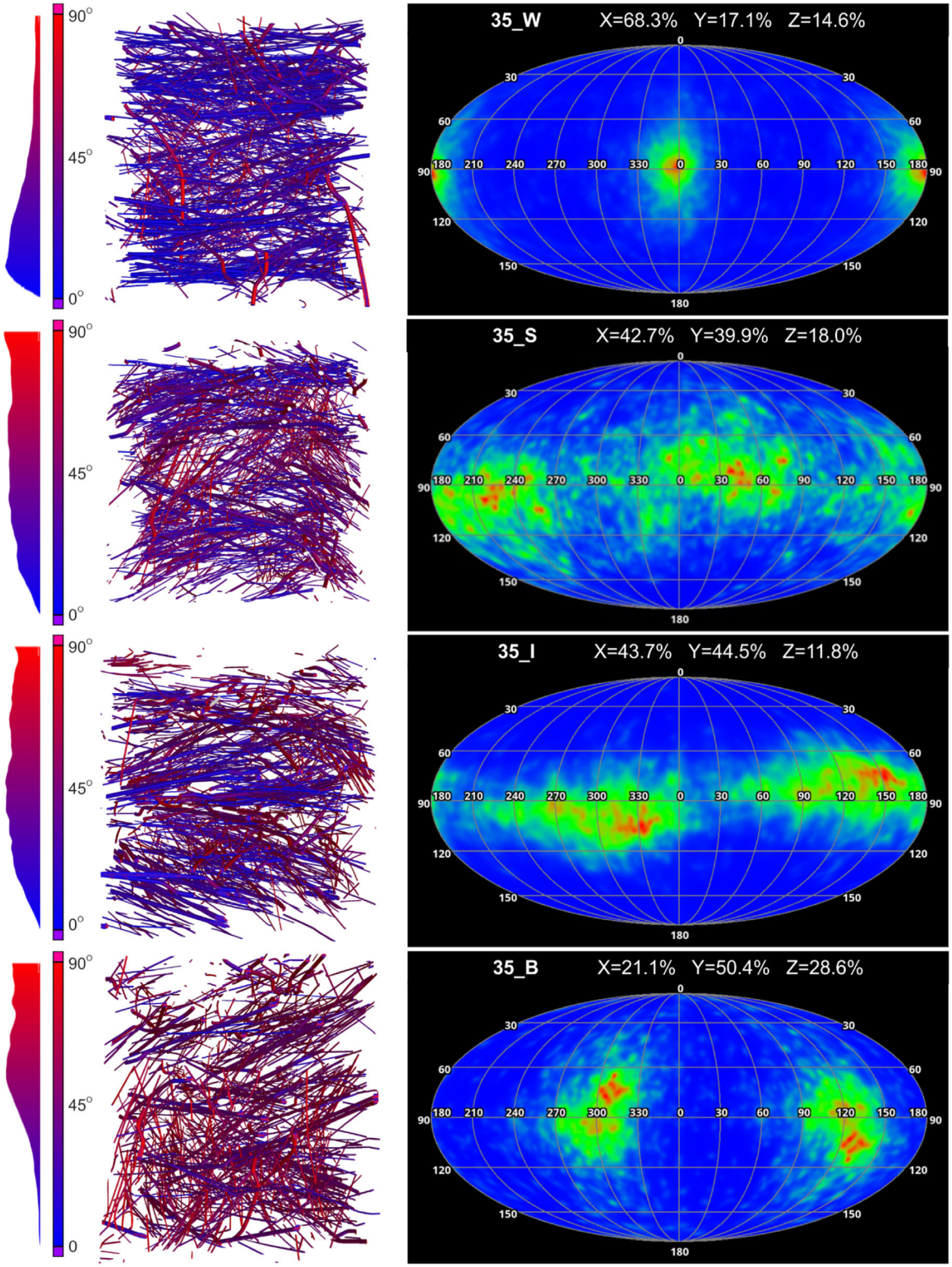
90°
45°
0°
35_W X=68.3% Y=17.1% Z=14.6%
35_S X=42.7% Y=39.9% Z=18.0%
35_I X=43.7% Y=44.5% Z=11.8%
35_B X=21.1% Y=50.4% Z=28.6%
0 30 60 90 120 150 180 210 240 270 300 330
(a)
(b)
(c)

◀**Fig. 8** Graphical result of CT performed on the specimens. **b** 3D segmented fibers color coded to deviation angles from *X* direction; **a** histogram of deviation angles (in blue are fibers directed along *X*); **c** equatorial plot of fiber orientation (on the blue planisphere, green areas are where fibers are oriented. Red areas mean a clustering of fiber orientations. Value of mean orientation in the three principal directions is also given)

X (longitudinal direction) is always found in the 35_W series, while badly oriented specimens have a preferred orientation along *Y* (the other planar direction during casting). The Z axis (vertical) has generally the lowest orientation values for all series. 35_S and 35_I always show an intermediate trend between well and badly oriented elements, but in the BSM100 results the 35_S series shows a slightly more pronounced orientation along *X* than 35_I. This is not the case for CT results, where the two series have very similar values. The reason for this lies in the different sample size between measuring methods; namely, for CT, only a 35 mm side cube in the center of the cross-section was analyzed, away from border effects caused by the formwork of the standard specimens. In this region of standard beams, the fiber orientation can be regarded as isotropic.

Figure 8 presents the outcome of CT analysis. Figure 8b shows the graphical representation of all fibers found in the volume, color coded to the angle of orientation with respect to the preferred *X* direction. Blue fibers are aligned with *X*, while red fibers lie in the plane perpendicular to *X*. It should be noticed that the well oriented specimen shows almost only blue fibers; this trend gradually changes by moving to the badly oriented specimen, where there is a wide majority of red colored fibers. Figure 8a shows a histogram depicting the totality of fibers divided according to the angle they form with the *X* direction. Once again, the histogram proves how the largest amount of fibers in the well oriented specimen have an angle smaller than 30° with respect to *X*. This trend is reversed for the badly oriented specimen, where almost no fibers are found in such range. As expected, 35_S and 35_I specimens show an approximately average distribution of orientations. In Fig. 8c, all fibers present in the volume are ideally positioned in the center of a sphere. The orientation of each fiber is represented by a coloring on the surface of such sphere. Green means one fiber, while red is a clustering of fiber orientations. The sphere is then represented as a planisphere. The longitudinal direction (*X*) is found on the equator at 0° and 180°. The other planar direction during casting (*Y*) is always on the equator, but at 90° and 270°, while the vertical direction during casting (*Z*) is at the poles of the planisphere. As an example, the 35_W specimen shows a red cluster exactly at 0° on the equator; this means that the majority of fibers are aligned along the longitudinal direction *X*.

4 Concluding remarks

In SFRC, many factors affect the post-cracking material performance which is of paramount importance for a SFRC structural element. Fiber orientation may be a problem if real mechanical performances are lower than those determined from standard tests but can be an opportunity if fiber orientation is managed during SFRC casting operations, since better mechanical performances could be obtained with a lower amount of fibers.

During the casting process, workability and viscosity of the mixture as well as flow and border effects are of paramount importance because, in turn, they affect fiber orientation.

In the present work, a wide range of fiber orientations in prismatic elements was tested to assess the impact of such factor on the residual flexural tensile strength. A device was specifically designed for the purpose of imparting a preferred uniaxial orientation to the fibers during the casting process, through vibration and a series of narrow channels, independent from the formwork borders. Specimens with fibers oriented parallel or perpendicular to the direction of tensile stresses expected during mechanical testing were made, producing a favorable or unfavorable orientation. Moreover, additional specimens were produced according to standard beams procedures required by EN 14651. The proposed device proved to effectively orient fibers.

From experimental results on 3-point bending beams (according to EN 14651), the following conclusions can be drawn:

- Specimens with well oriented fibers have a slightly higher residual tensile strength than standard beams cast according to EN 14651, which is the basis for defining SFRC strength classes.

- Beams with an isotropic fiber orientation have a lower average residual tensile strength, up to -41%, than beams cast according to EN 14651.
- Beams with badly oriented fibers have a much lower average residual tensile strength, up to 61% lower than beams cast according to EN 14651.

Moreover, the fiber orientation in cubes extracted from the tested beams was experimentally determined through the ferromagnetic induction instrument BSM100; such correlation is confirmed by computed tomography analysis of samples from each orientation pool. It was observed that post-cracking strength values are almost linearly dependent on the percentage of fibers oriented in the direction of the stresses present in bending tests.

These results underline the importance of the orientation factor for structural design of FRC structural elements, since standard beams, especially with longer fibers (that are more prone to wall effects), have mechanical post-cracking performances similar to specimens with well oriented fibers. At the same time, fiber orientation may represent an opportunity, if well managed, to optimize the material performance.

Acknowledgements The authors gratefully acknowledge the help of Prof. Rolf Breitenbücher in the development of the concrete mix design, and the precise and dedicated work of the members of the Structural Testing Laboratory (KIBKON) at Ruhr University Bochum.

Funding Open Access funding enabled and organized by Projekt DEAL. No funding was received for conducting this study.

Declarations

Conflict of interest The authors declare that they have no conflict of interest.

References

1. Edgington J, Hannant D (1972) Steel fibre reinforced concrete. The effect on fibre orientation of compaction by vibration. Mater Struct 5(1):41–44. https://doi.org/10.1016/0010-4361(72)90102-4
2. Soroushian P, Lee CD (1990) Distribution and orientation of fibers in steel fiber reinforced concrete. ACI Mater J 87(5):433–439
3. di Prisco M, Plizzari G, Vandewalle L (2009) Fibre reinforced concrete: new design perspectives. Mater Struct 42(9):1261–1281. https://doi.org/10.1617/s11527-009-9529-4
4. DAfStb (2012) Guideline for steel fibre reinforced concrete. Berlin
5. fib (2013) Model code for concrete structures 2010. Ernst & Sohn, Lausanne. ISBN: 978-3-433-03061-5
6. Smarslik M, Mark P (2019) Hybrid reinforcement design of longitudinal joints for segmental concrete linings. Struct Concr 20(6):1926–1940. https://doi.org/10.1002/suco.201900081
7. Trabucchi I, Smarslik M, Tiberti G et al (2021) A hybrid solution proposal for precast tunnel segments. Struct Concr 22(3):1534–1548. https://doi.org/10.1002/suco.202000629
8. Belletti B, Cerioni R, Meda A et al (2008) Design aspects on steel fiber-reinforced concrete pavements. J Mater Civ Eng 20(9):599–607. https://doi.org/10.1061/(ASCE)0899-1561(2008)20:9(599)
9. Ferrara L, Meda A (2006) Relationships between fibre distribution, workability and the mechanical properties of SFRC applied to precast roof elements. Mater Struct 39:411–420. https://doi.org/10.1617/14247
10. Dupont D, Vandewalle L (2005) Distribution of steel fibres in rectangular sections. Cem Concr Compos 27(3):391–398. https://doi.org/10.1016/j.cemconcomp.2004.03.005
11. Laranjeira F, Aguado A, Molins C et al (2012) Framework to predict the orientation of fibers in FRC: a novel philosophy. Cem Concr Res 42(6):752–768. https://doi.org/10.1016/j.cemconres.2012.02.013
12. Boulekbache B, Hamrat M, Chemrouk M et al (2010) Flowability of fibre-reinforced concrete and its effect on the mechanical properties of the material. Constr Build Mater 24(9):1664–1671. https://doi.org/10.1016/j.conbuildmat.2010.02.025
13. Alberti MG, Enfedaque A, Gálvez JC (2018) A review on the assessment and prediction of the orientation and distribution of fibres for concrete. Compos Part B: Eng 151:274–290. https://doi.org/10.1016/j.compositesb.2018.05.040
14. Gettu R (2005) Study of the distribution and orientation of fibers in SFRC specimens. Mater Struct 38(275):31–37. https://doi.org/10.1617/14021
15. Alberti MG, Enfedaque A, Gálvez JC (2017) On the prediction of the orientation factor and fibre distribution of steel and macro-synthetic fibres for fibre-reinforced concrete. Cem Concr Compos 77:29–48. https://doi.org/10.1016/j.cemconcomp.2016.11.008
16. Maryamh K, Hauch K, Redenbach C et al (2021) Influence of production parameters on the fiber geometry and the mechanical behavior of ultra high performance fiber-reinforced concrete. Struct Concr 22(1):361–375. https://doi.org/10.1002/suco.202000105

17. Look K, Mark P (2022) Steel fiber reinforced concrete tensile testing with eliminated lateral wall effect. Struct Concr. https://doi.org/10.1002/suco.202100831
18. Maryamh K, Hauch K, Redenbach C et al (2022) Influence of specimen size on the fibre geometry and tensile strength of ultra-high-performance fibre-reinforced concrete. Struct Concr 23(2):1239–1252. https://doi.org/10.1002/suco.202000753
19. Stähli P, Custer R, van Mier JGM (2008) On flow properties, fibre distribution, fibre orientation and flexural behaviour of FRC. Mater Struct 41(1):189–196. https://doi.org/10.1617/s11527-007-9229-x
20. Zerbino R, Tobes JM, Bossio ME et al (2012) On the orientation of fibres in structural members fabricated with self compacting fibre reinforced concrete. Cem Concr Compos 34(2):191–200. https://doi.org/10.1016/j.cemconcomp.2011.09.005
21. Torrijos MC, Barragán BE, Zerbino RL (2010) Placing conditions, mesostructural characteristics and post-cracking response of fibre reinforced self-compacting concretes. Constr Build Mater 24(6):1078–1085. https://doi.org/10.1016/j.conbuildmat.2009.11.008
22. Look K, Heek P, Mark P (2021) Towards rebar substitution by fibres—tailored supercritical fibre contents. In: Serna P, Llano-Torre A, Martí-Vargas JR et al. (eds) BEFIB 2020. Improvements and innovations: RILEM-fib international symposium on FRC, vol 30. Springer, Cham, pp 908–919
23. Mu R, Li H, Qing L et al (2017) Aligning steel fibers in cement mortar using electro-magnetic field. Constr Build Mater 131:309–316. https://doi.org/10.1016/j.conbuildmat.2016.11.081
24. Hajforoush M, Kheyroddin A, Rezaifar O (2020) Investigation of engineering properties of steel fiber reinforced concrete exposed to homogeneous magnetic field. Constr Build Mater 252:119064. https://doi.org/10.1016/j.conbuildmat.2020.119064
25. EN 14651:2005+A1 (2007) Test method for metallic fibre concrete-Measuring the flexural tensile strength (limit of proportionally (LOP), residual). European Committee for Standardization (CEN), Brussels
26. Žirgulis G, Švec O, Sarmiento EV et al (2015) Importance of quantification of steel fibre orientation for residual flexural tensile strength in FRC. Mater Struct 49(9):3861–3877. https://doi.org/10.1617/s11527-015-0759-3
27. Leutbecher T, Rebling J (2019) Predicting the postcracking strength of ultra-high performance fiber reinforced concrete by means of three-point bending tests according to EN 14651. Struct Concr 20(6):2081–2095. https://doi.org/10.1002/suco.201900070
28. Žirgulis G, Švec O, Geiker MR et al (2016) Variation in fibre volume and orientation in walls: experimental and numerical investigations. Struct Concr 17(4):576–587. https://doi.org/10.1002/suco.201500060
29. Conforti A, Cuenca E, Zerbino R et al (2021) Influence of fiber orientation on the behavior of fiber reinforced concrete slabs. Struct Concr 22(3):1831–1844. https://doi.org/10.1002/suco.202000612
30. Leporace-Guimil B, Mudadu A, Conforti A et al (2022) Influence of fiber orientation and structural-integrity reinforcement on the flexural behavior of elevated slabs. Eng Struct 252:113583. https://doi.org/10.1016/j.engstruct.2021.113583
31. Mudadu A, Tiberti G, Germano F et al (2018) The effect of fiber orientation on the post-cracking behavior of steel fiber reinforced concrete under bending and uniaxial tensile tests. Cem Concr Compos 93:274–288. https://doi.org/10.1016/j.cemconcomp.2018.07.012
32. Song F (2017) Steel fiber reinforced concrete under concentrated load. Dissertation, Ruhr University Bochum
33. Plückelmann S, Breitenbücher R, Smarslik M et al (2019) Aufnehmbare teilflächenspannung von hochfestem stahlfaserbeton. Beton- und Stahlbetonbau 114(9):653–662. https://doi.org/10.1002/best.201900015
34. EN 12350-5:2019 (2019) Testing fresh concrete–Part 5: flow table test. European Committee for Standardization (CEN), Brussels
35. Medeghini F, Plizzari GA, Mark P (2022) Steering fiber orientation in concrete for structural applications. In: di Prisco M, Meda A, Balazs GL (eds) 14th fib PhD symposium in civil engineering, Rome, pp 729–736
36. Grünewald S (2004) Performance-based design of self-compacting fibre reinforced concrete. Dissertation Delft University of technology
37. Trabucchi I, Tiberti G, Conforti A et al (2021) Experimental study on Steel fiber reinforced concrete and reinforced concrete elements under concentrated loads. Constr Build Mater 307:124834. https://doi.org/10.1016/j.conbuildmat.2021.124834
38. Faccin E, Facconi L, Minelli F et al. (2022) Predicting the residual flexural strength of concrete reinforced with hooked-end steel fibers: new empirical equations. In: Serna P, Llano-Torre A, Martí-Vargas JR et al. (eds) BEFIB 2021. Fibre reinforced concrete: improvements and innovations II. X RILEM-Fib international symposium on fibre reinforced concrete, vol 36. Springer, pp 456–468
39. Tiberti G, Germano F, Mudadu A et al (2017) An overview of the flexural post-cracking behavior of steel fiber reinforced concrete. Struct Concr 19(3):695–718. https://doi.org/10.1002/suco.201700068
40. Wichmann H-J, Holst A, Budelmann H (2013) Ein praxisgerechtes messverfahren zur bestimmung der fasermenge und -orientierung im stahlfaserbeton. Beton- und Stahlbetonbau 108(12):822–834. https://doi.org/10.1002/best.201300060
41. Martinelli P, Colombo M, Pujadas P et al. (2021) Characterization tests for predicting the mechanical performance of SFRC floors: identification of fibre distribution and orientation effects. Mater Struct. https://doi.org/10.1617/s11527-020-01593-7
42. Ferrara L, Ozyurt N, di Prisco M (2011) High mechanical performance of fibre reinforced cementitious composites: the role of "casting-flow induced" fibre orientation. Mater Struct 44(1):109–128. https://doi.org/10.1617/s11527-010-9613-9
43. Du Plessis A, Olawuyi BJ, Boshoff WP et al (2016) Simple and fast porosity analysis of concrete using X-ray computed tomography. Mater Struct 49(1–2):553–562. https://doi.org/10.1617/s11527-014-0519-9
44. Rettinger M, Guhathakurta J, Gänz P et al (2022) Hinter den Kulissen. Beton- und Stahlbetonbau 117(5):343–356. https://doi.org/10.1002/best.202200008

45. Lee H-J, Seo E-A, Kim W-W et al. (2021) X-ray CT analysis of the cross-section of a 3D-printed deformed layer. Mater. https://doi.org/10.3390/ma14247764
46. Vicente MA, González DC, Mínguez J (2019) Recent advances in the use of computed tomography in concrete technology and other engineering fields. Micron 118:22–34. https://doi.org/10.1016/j.micron.2018.12.003
47. Ponikiewski T, Katzer J, Bugdol M et al (2015) Steel fibre spacing in self-compacting concrete precast walls by X-ray computed tomography. Mater Struct 48(12):3863–3874. https://doi.org/10.1617/s11527-014-0444-y
48. Schönlin K (1988) Ermittlung der orientierung, menge und verteilung der fasern in faserbewehrtem beton. Beton- und Stahlbetonbau 83(6):168–171. https://doi.org/10.1002/best.198800280
49. Advani SG, Tucker CL (1987) The use of tensors to describe and predict fiber orientation in short fiber composites. J Rheol 31(8):751–784. https://doi.org/10.1122/1.549945